PERFORMANCES OF SILICON-BASED FIELD-EMISSION CATHODES COATED WITH ULTRANANO CRYSTALLINE DIAMOND*

O. Mohsen[1†], A. Lueangaramwong[1], S. Valluri[1], R. Divan[2],
V. Korampally[1], A. Sumant[2], P. Piot[1,3],
[1] Northern Illinois University, DeKalb, IL 60115, USA
[2] Argonne National Laboratory, Argonne, IL 60439, USA
[3] Fermi National Accelerator Laboratory, Batavia, IL 60510, USA

Abstract

Field-emission electron sources have been considered as possible candidates for the production of bright or high-current electron bunches. In this paper, we report on the experimental characterization of silicon-based field-emitter arrays (FEA) in a DC high voltage gap. The silicon cathodes are produced via a simple self-assembling process. The measurement reported in this paper especially compares the field-emission properties of a nanostructured and planar diamond-coated Si-based cathode.

INTRODUCTION

Field Emission (FE) [1], i.e., the macroscopic manifestation of electron tunneling through a potential barrier associated with a surface subjected to a high electric field, offers a promising alternative to other electron-emission mechanisms. FE can originate from nanoscale single emitters and is capable of supporting the emission of bright close-to-quantum-degenerate electron beams. Likewise, structured cathodes consisting of a large number of such emitters [arranged as "field-emitter arrays" (FEAs)] provide a path toward the realization of rugged high-current electron sources. In the latter application, one of the advantages of FE is its natural bunching in the presence of a time-dependent electric field [2]. The FE process is classically described by the Fowler-Nordheim (F-N) equation [1]

$$ j = A(\phi)[\beta_e E]^2 \, \mathrm{e}^{\frac{-B(\phi)}{\beta_e E}}, \tag{1} $$

where $A(\phi)$ and $B(\phi)$ depend on the work function ϕ of the material, β_e is the field enhancement factor and E is the applied electric field. This paper reports on experimental measurements of FEAs made from nano-engineered Si cathodes. We especially explore the impact of coating the cathode with a Nitrogen doped ultra-nano-crystalline diamond (N-UNCD) layer [3, 4].

EXPERIMENTAL SETUP

The experiments were performed in an ultra-high vacuum (UHV, $\sim 10^{-8}$ Torr) DC gap diagrammed in Fig. 1. The FE cathode is glued on a grounded staleness steal mount using conductive UHV-compatible epoxy (from Accu-Glass Products, Inc). An insulating cylindrical spacer made from Polyphenylene sulfide (from Techtron ®), is used to control the gap between the anode and the cathode. The part of the spacer facing the anode has a smaller inner diameter of thereby covering the edges of the cathode to avoid possible spurious emission from the peripheral region of the silicon wafer.
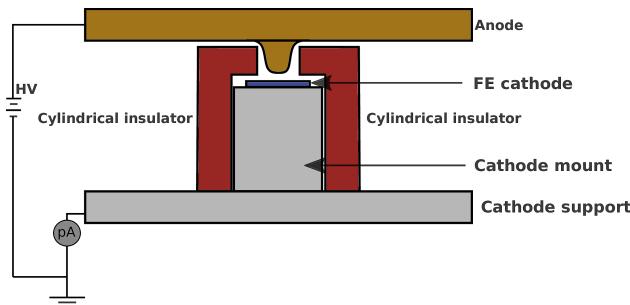

Figure 1: Schematic of the setup used in our experiments. The anode-cathode gap can be varied by changing the cylindrical insulator.

Cylinders with different lengths (100 μm to 500 μm) were machined to provide a way to change the cathode-anode gap size. A high voltage (HV) power supply (Model:PS375 by Stanford Research Systems) is used to apply a voltage between the cathode and the anode. The current is recorded using a picoammeter (Model:6485 by Keithley). More technical details about the setup are available in Ref. [5].

In this paper, we considered two cathodes. Both cathodes consist of an n-type ⟨111⟩ Silicon-wafer base coated with Nitrogen-doped UNCD (N-UNCD). The referenced cathode consists of an N-UNCD-coated planar Si wafer (henceforth referred to as "Planar") while the other cathode is nano-engineered to provide an ordered FEA consisting of sharp tips with sub-micron periods (henceforth referred to as "FEA cathode"). The FEA cathode is prepared from self-assembled monolayers of 1.18 μm Silica spheres deposited on the Si wafer. The spheres form a mask to structure the wafer via etching processes. A first anisotropic profile is performed with chlorine. A reactive-ion etching process
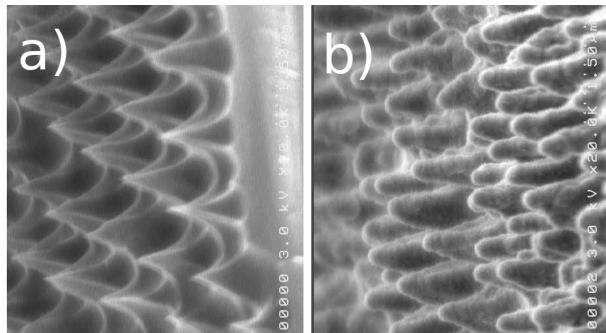
Figure 2: Scanning electron microscopy (SEM) micrograph Silicon FEA before (a) and after (b) the UNCD deposition.

is then achieved using an Ar/SF6 composition of gases to create an isotropic etch profile. Finally, the silicon tips are formed via thermal oxidation; see Fig. 2(a). Silicon emitters are coated with Nitrogen-doped UNCD (N-UNCD) [3,6]. The cathodes are then coated with a 25 nm layer of tungsten which acts as an adhesive for the diamond. The N-UNCD is deposited using microwave plasma chemical vapor deposition (MPCVD); see Fig. 2(b) for the resulting N-UNCD Si-tip FEA. It should be noted that the UNCD deposition leads to a significant decrease in the sharpness of the tips (the radius of curvature of the tips typically increases from ~ 30 to ~ 100 nm).

RESULTS

The two cathodes discussed in the previous section were characterized in the diode set up. For each sample, several $I - V$ characteristic curves were measured: the applied voltage is gradually increased and for each set point, the emitted current is recorded 10 times so to compute an average current and its standard deviation. The $I-V$ characteristic curve are recorded following the sequence $V_{min} \rightarrow V_{max} \rightarrow V_{min}$ where V_{min} (resp. V_{max}) are the minimum (resp. maximum) value for the set voltage. During the measurements, the vacuum pressure did not appreciably deteriorate and remained at levels of 10^{-7} to 10^{-9} Torr. In the case of the FEA sample, the $I - V$ curves were recorded for two anode-cathode spacing (200 µm and 300 µm).

While for the planar cathode only the smaller gap could be used.

Figure 3 shows the averaged $I - V$ curves for the FEA sample with 2 different anode-cathode spacing. The voltage range is chosen such that the macroscopic filed ($E = V/d$) is the same for both anode-cathode spacings. In the case of the 300 µm anode-cathode gap, higher voltage is required to achieve the same macroscopic fields when compared to the 200 µm anode-cathode case. Increasing the voltage higher than 8.5 kV resulted in arcing, possibly due to some vacuum events. These arcing points were manually removed and not included Fig.3.

Figure 4 shows the average $I - V$ curved obtained for the planar UNCD sample. Unfortunately, the data for the larger spacing could not be recorded due to significant arcing. A
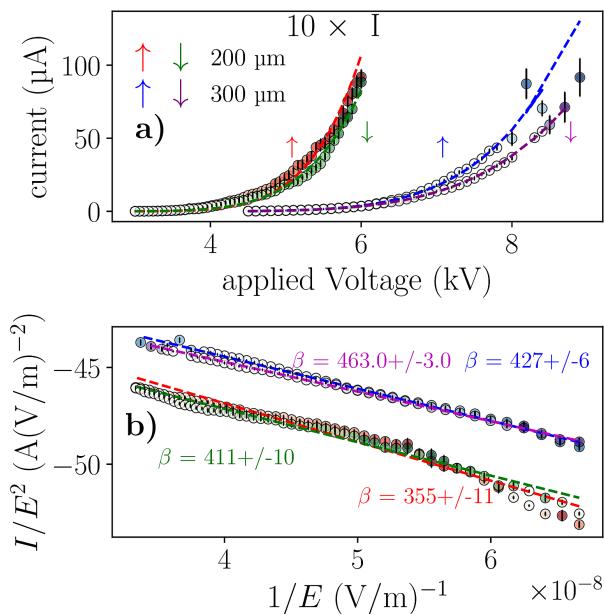

Figure 3: $I - V$ characteristic curve (a) and the associated F-N plot (b) for the FEA cathode. The traces corresponds to 200 µm (red and green traces) and 300 µm (blue and purple traces). The dashed line represents weighted least square fitting. The current for the case of 200 µm has been multiplied by 10 for clarity. The ↑ (resp. ↓) corresponds to an increasing (resp. decreasing) voltage.
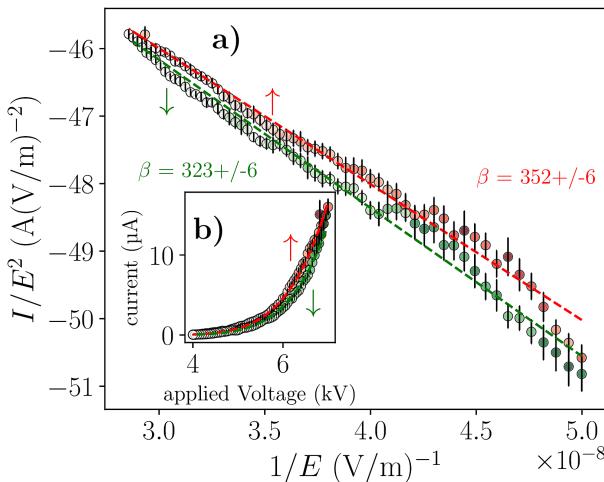

Figure 4: F-N plot for the planar sample (a) with inset (b) showing the $I - V$ characteristic curve. The measurement are performed for an anode-cathode spacing of 200 µm. See Fig. 3 for explanation of arrows and dashed lines.

post-mortem inspection of the cathode shows some damages (burn marks).

We observe that the FEA current increased by an order of magnitude when the gap spacing was raised from 200 to 300 µm. The origin for such an increase is currently not understood (note that the 300 µm data were taken after the

200 µm so possible damage to the cathode is eliminated). In fact, as the gap increases, we expect the emitting area to reduce due to field reduction at the periphery and WARP [7] simulations indicate the current would actually be ~ 10% larger for the 200 µm gap compared to the 300 µm case. Likewise, the possibility of space-charge-saturated emission was ruled out from a simple estimate and confirmed via numerical simulations.

The current stability and cathode lifetime were also explored by recording the current at a fixed voltage over several ~ 6-hour-long periods for both cathodes; see Fig. 5. The associated relative rms current variation for Fig. 5(a-c) are 22, 26 and 17%. During the recording of these curves, some arcs occurred and most likely occur some of the large variations. Likewise, the fast variation is attributed to vacuum processing in the anode-cathode gap.

Table 1: Field-enhancement factor β and effective emission area A_e for FEA and planar cathodes. The quantities β and A_e are written as Y $\pm$ χ $\pm$ η. The uncertainty χ correspond only include current variation while η also incorporates uncertainty in the work function $\phi = 4.9 \pm 1.0$ eV propagated through the analysis.

sample	spacing (µm)	β	A_e 10^{-16} (m²)
FEA ↑	200	355 ± 11 ±109	1.6 ± 0.5 ±0.72
FEA ↓	200	411± 10 ±126	0.31 ± 0.065 ± 0.12
FEA ↑	300	427 ± 6 ± 131	3.2 ± 0.42 ±1.1
FEA ↓	300	463 ± 3 ± 142	1.3 ± 0.07 ± 0.4
planar ↑	200	352 ± 6 ± 108	0.56 ± 0.09 ± 0.19
planar ↓	200	323 ± 6 ± 99	0.96 ± 0.16 ± 0.34

appear as lines with slope $m(\phi,\beta)$ and intercept $c(\phi,\beta,A_e)$ indirectly providing the values of β and A_e for an assumed work function value. In our analysis we consider a work function of $\phi = 4.9 \pm 1.0$ eV and the uncertainties on β and A_e were obtained using the python-based UNCERTAINTIES error-propagation package [8]. Such an analysis was performed with the data presented in Fig. 3(b) and 4(a) and the retrieved β and A_e parameters are summarized in Table 1.

Comparing the two cathodes for the same anode-cathode gap supports our earlier observations. We find that the β values are similar for the FEA and planar cathode which indicate the field-emission process is most likely dominated by the UNCD structure (an earlier measurement on a bare FEA with similar geometry give $\beta \sim 50$). Likewise, we generally find that the effective area recovered from the fit is larger for the FEA than for the planar cathode. From simple geometric consideration, we expect the area enhancement to be ~ 3 which qualitatively agrees with our measurements.
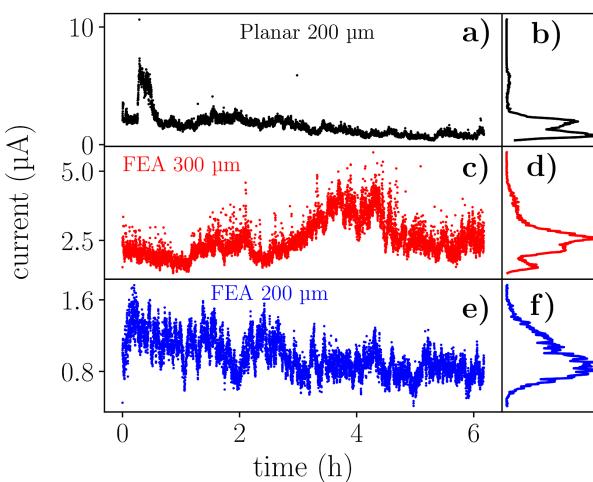

Figure 5: Long term stability test for the planar (a) and FEA (c and e) samples and the associated histogram for the obtained current (b,d and f). In the case of the FEA cathode the stability test was performed under the same applied field ($E = V/d$) of $20\,\text{MV}\,\text{m}^{-1}$, while for the planar cathode, the field is $30\,\text{MV}\,\text{m}^{-1}$.

DISCUSSION & ANALYSIS

From the $I - V$ characteristic, we can extract some of the parameters associated with the field emission process. Considering the F-N law written as

$$I = \frac{1.54 \times 10^{-6} \times 10^{4.52\frac{1}{\sqrt{\phi}}} A_e \beta^2 E^2}{\phi}$$
$$\times \exp\left(\frac{-6.53 \times 10^9 \phi^{1.5}}{\beta E}\right) \qquad (2)$$

where A_e is the effective emission area (defined as the sum of the emitting area associated with each field emitter), and the applied macroscopic electric field E is related to the applied voltage by $E = V/d$, where d is the anode-cathode gap. The $I - V$ data are reported on a F-N plot where they

CONCLUSION

We have explored field emission from a planar and FEA cathodes consisting of a Silicon substrate and coated with a UNCD layer. Our preliminary data indicate that both cathodes have comparable effective emission areas ~ 10^{-16} m² along with similar field-enhancement factors. The measurements indicate the emission is dominated by the UNCD structure (i.e. the emission is dominated by grain boundaries in the UNCD layer rather than sharp edges associated with the FEA), and that the slight increase in current is most likely due to an increase in surface owing to the conical shape of the emitted constituting the FEA cathode.

In the near future, we plan on performing further measurements to systematically compare the bare FEA, with an UNCD-coated FEA and the planar UNCD cathode to examine the reproducibility of the measurements in this paper.

REFERENCES

[1] R. H. Fowler and L. Nordheim, "Electron emission in intense electric fields," in *Proc. Roy. Soc. London A*, vol. 119, pp. 173–181, The Royal Society, 1928.

[2] P. Piot, C. Brau, B. Choi, B. Blomberg, W. Gabella, B. Ivanov, J. Jarvis, M. Mendenhall, D. Mihalcea, H. Panuganti, and P. Prieto, "Operation of an ungated diamond field-emission array cathode in a l-band radiofrequency electron source," *Appl. Phys. Lett.*, vol. 104, no. 26, p. 263504, 2014.

[3] A. Krauss, O. Auciello, M. Ding, D. Gruen, Y. Huang, V. Zhirnov, E. Givargizov, A. Breskin, R. Chechen, E. Shefer, *et al.*, "Electron field emission for ultrananocrystalline diamond films," *Journal of Applied Physics*, vol. 89, no. 5, pp. 2958–2967, 2001.

[4] S. V. Baryshev, S. Antipov, J. Shao, C. Jing, K. J. Pérez Quintero, J. Qiu, W. Liu, W. Gai, A. D. Kanareykin, and A. V. Sumant, "Planar ultrananocrystalline diamond field emitter in accelerator radio frequency electron injector: Performance metrics," *Applied Physics Letters*, vol. 105, no. 20, p. 203505, 2014.

[5] O. Mohsen, A. Lueansaramwong, S. Valluri, V. Korampally, P. Piot, and S. Chattopadhyay, "Field emission from silicon nanocones cathodes," in *2018 IEEE Advanced Accelerator Concepts Workshop (AAC)*, pp. 1–5, IEEE, 2018.

[6] W. Choi, J. Cuomo, V. Zhirnov, A. Myers, and J. Hren, "Field emission from silicon and molybdenum tips coated with diamond powder by dielectrophoresis," *Applied physics letters*, vol. 68, no. 5, pp. 720–722, 1996.

[7] A. Friedman, R. H. Cohen, D. P. Grote, S. M. Lund, W. M. Sharp, J.-L. Vay, I. Haber, and R. A. Kishek, "Computational methods in the warp code framework for kinetic simulations of particle beams and plasmas," *IEEE Trans. Plasma Sci.*, vol. 42, no. 5, pp. 1321–1334, 2014.

[8] E. O. LEBIGOT, "Uncertainties: a python package for calculations with uncertainties."